

S.M. Aarons

**Variable Hf-Sr-Nd radiogenic isotopic compositions in a Saharan dust storm over the Atlantic:  
Implications for dust flux to oceans, ice sheets and the terrestrial biosphere**

Submitted for Publication in:

*Chemical Geology*

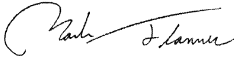
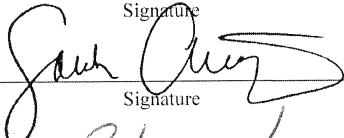
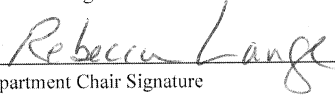
in lieu of thesis in partial fulfillment of the requirements for the degree of

**Master of Science in Geology**

Department of Earth and Environmental Sciences

The University of Michigan

Accepted by:

 Signature	Mark Flanner	11-Dec-2012
_____ Name	_____ Date	
 Signature	Sarah M. Aciego	12/11/2012
_____ Name	_____ Date	
 Department Chair Signature	Rebecca Lange	12/12/2012
_____ Name	_____ Date	

I hereby grant the University of Michigan, its heirs and assigns, the non-exclusive right to reproduce and distribute single copies of my thesis, in whole or in part, in any format. I represent and warrant to the University of Michigan that the thesis is an original work, does not infringe or violate any rights of others, and that I make these grants as the sole owner of the rights to my thesis. I understand that I will not receive royalties for any reproduction of this thesis.

- Permission granted.
- Permission granted to copy after: \_\_\_\_\_
- Permission declined.



Author Signature

**Earth and Environmental Sciences**  
**M** UNIVERSITY OF MICHIGAN

# Variable Hf-Sr-Nd radiogenic isotopic compositions in a Saharan dust storm over the Atlantic: Implications for dust flux to oceans, ice sheets and the terrestrial biosphere

S.M. Aarons, S.M. Aciego and J.D. Gleason

*S. M. Aarons (smaarons@umich.edu), S.M. Aciego, and J.D. Gleason, Department of Earth and Environmental Sciences, University of Michigan, 2534 C.C. Little Building, Ann Arbor, MI 48109, USA.*

---

## Abstract

Isotopic characterization of aerosol mineral particles (atmospheric dust) of varying sizes is essential in classifying source areas, and for determining the source of dust deposited over oceans and ice sheets. However, the effect of atmospheric transport on radiogenic isotopic compositions is not well constrained, making provenance interpretation difficult. In order to investigate the isotopic variability of  $^{176}\text{Hf}/^{177}\text{Hf}$ ,  $^{87}\text{Sr}/^{86}\text{Sr}$  and  $^{143}\text{Nd}/^{144}\text{Nd}$  we analyzed eight airborne dust samples in two size fractions collected along a cross-Atlantic transect through a dust storm originating in the Sahara in late 2002. Past measurements of  $^{176}\text{Hf}/^{177}\text{Hf}$ ,  $^{87}\text{Sr}/^{86}\text{Sr}$  and  $^{143}\text{Nd}/^{144}\text{Nd}$  of dust have focused primarily on coarse sized particles ( $<30\ \mu\text{m}$ ), whereas far field deposition is primarily finer particles ( $<2\ \mu\text{m}$ ). Strontium or neodymium isotopic sorting based on distance is not evident in our dataset; however, the combined isotopic ratios of the dust collected suggests a Saharan origin. Hafnium isotopic compositions show an east to west trend towards more radiogenic compositions across the Atlantic, suggesting grain and mineral sorting during dust transport along the  $\sim 4000\ \text{km}$  transect. Transport models with variable dust particle diameter and wind speed demonstrate that the Hf isotopic compositions can be explained by the loss of the high-density mineral zircon during transport of dust from the source area. Modeling of this “zircon effect” in the Hf isotopic composition of marine, terrestrial and glacial dust deposits can reveal additional information concerning dust transport and sources in the geologic past.

*Keywords:* Dust, Hf, Sr, Nd, Zircon Effect

---

## 1. Introduction

The Sahara desert (Fig. 1) is considered the primary source of aerosol dust in the Northern Hemisphere (Sarnthein et al., 1981; Duce et al., 1991). Saharan dust is transported thousands of kilometers across the Atlantic and has been recognized as a nutrient source with a significant impact on ocean-carbon dynamics (Watson et al., 2000) and the ecosystems of the southeastern United States and the Caribbean (Prospero, 1999; Shinn et al., 2000). Dust particles originating from desert areas and deposited in ice sheets have also been used as tracers of atmospheric circulation and transport patterns (Genthon et al., 1993; Joussaume et al., 1993; Basile et al., 1997). Comparing the composition of dust particles entrained in ice to that of dust particles from known dust sources such as the Sahara desert can effectively trace back the origin of dust from sink to source (Grousset and Biscaye, 2005). Radiogenic isotope tracers allow us to more fully

*Preprint submitted to Chemical Geology*

*December 10, 2012*

investigate the impact of a dust source on oceanic and terrestrial biogeochemistry, and provide insight on paleo-atmospheric circulation and paleo-climate (Grousset et al., 1992; Harrison et al., 2001; Jickells et al., 2005). Effective quantification and modeling of the isotopic data assumes that we understand changes in isotope composition occurring as a result of weathering, transport, deposition and dissolution. Previous studies have assumed the isotopic composition of dust particles remains the same between source and sink despite the possibility of fractionation effects during transport (Grousset and Biscaye, 2005). Here, we quantify some specific effects that transport can have on the radiogenic isotopic composition of varying sizes of aerosol dust by investigating a dust storm event originating in the Sahara desert in 2002.

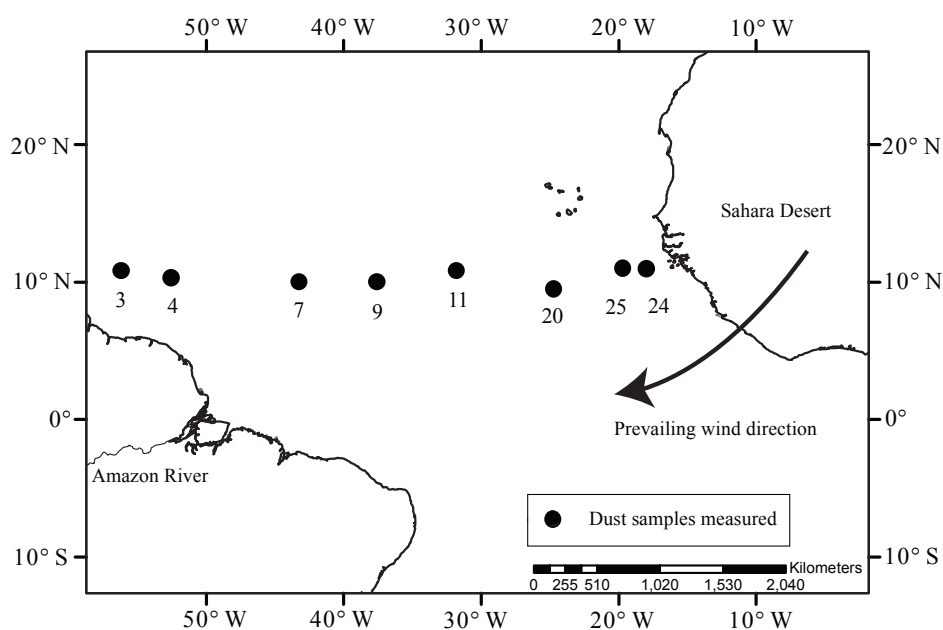


Figure 1: Map of Atlantic Ocean with locations of aerosol dust sample collection sites during cruise M55. Collection sites listed are the samples that were measured in this study.

## 2. Methodology

### 2.1. Sample processing

Aerosol dust samples were collected on shipboard filters during Atlantic cruise M55 of FS Meteor (Curacao, West Indies to Douala, Cameroon, 12th October-17th November 2002), which intersected a cross-Atlantic dust storm originating in the Sahara desert (Fig. 1). The distance between the first dust collection point and the last collection point is over 4000 km, with samples approximately 500 to 1000 km apart (Fig. 1). The distance for the most westerly sample from the dust source is estimated to be nearly 6000 km. Aerosol samples were collected using a high volume ( $1 \text{ m}^3 \text{ min}^{-1}$ ) collector which separated the dust into two size fractions,  $<1$  and  $>1 \mu\text{m}$  with a maximum particle size of  $30 \mu\text{m}$ . Filters were changed approximately once a day and the average air volume sampled was  $\sim 1400 \text{ m}^3$  (Baker, 2004). Dust was separated from

the filters under Class 100 clean lab conditions by ultrasonic bath with Super-Q Millipore water. Following centrifugation, the water was decanted and retained for analysis of the water-soluble portion of the samples. The water-insoluble dust fraction was transferred to pre-cleaned Savillex Teflon vials and digested in aqua regia, dried and re-digested in ultra-pure double distilled Seastar HF/HNO<sub>3</sub>/HClO<sub>4</sub> for >24 hours at 160°C before evaporation. Following evaporation and uptake in Seastar HCl, sample solutions were inspected for any residues. Clear solutions were further processed and chemically separated by ion exchange chromatography using miniaturized ion-exchange columns and Eichrom resins following techniques of Aciego et al. (2009) for Hf, Sr and Nd isotopic analysis. The water-soluble fraction was also recovered, and then chemically separated using the same methodology.

## 2.2. Mass spectrometry

Strontium isotopic compositions were measured on a Finnigan MAT 262 thermal ionization mass spectrometer and normalized to  $^{88}\text{Sr}/^{86}\text{Sr}=8.375209$  to correct for mass bias. The Sr isotopic standard NBS987 (75 ng) has a long term average of  $^{87}\text{Sr}/^{86}\text{Sr}=0.710235\pm 12$  ( $2\sigma$  SD,  $n = 88$ ) on the University of Michigan Finnigan MAT 262. The USGS reference material BCR-2 (10 ng) measured at the same time as the samples averaged  $0.705002\pm 30$  ( $n = 4$ ), which is in good agreement with the literature value compiled in Aciego et al. (2009) (0.705013). Hafnium isotopic measurements were performed on the University of Michigan Nu Instruments multi-collector inductively coupled mass spectrometer and ratios were normalized to  $^{179}\text{Hf}/^{177}\text{Hf}=0.7325$ . Samples were bracketed with a standard solution of JMC475 (20 ppb total Hf) which had an average  $^{176}\text{Hf}/^{177}\text{Hf}=0.282170\pm 22$  ( $n = 24$ );  $^{176}\text{Hf}/^{177}\text{Hf}$  of the samples were then normalized to the accepted JMC475 value of 0.282160 (Weis et al., 2007). BCR-2 solutions were measured twice for Hf isotopic composition, and the average value ( $^{176}\text{Hf}/^{177}\text{Hf}=0.282886$ ;  $\epsilon_{\text{Hf}}=4.13$ ), is in close agreement with literature values (Weis et al., 2007). Our reported  $^{87}\text{Sr}/^{86}\text{Sr}$  errors represent individual analytical errors, whereas the  $^{176}\text{Hf}/^{177}\text{Hf}$  errors are based on our external reproducibility of the standard JMC475. Neodymium isotopic compositions were measured on a Thermo Scientific Triton PLUS thermal ionization mass spectrometer at the University of Michigan and normalized to  $^{146}\text{Nd}/^{144}\text{Nd}=0.7219$  using the exponential law and mass 149 was monitored for Sm interference. The Nd isotopic standard JNdi-1 (10 ng) was measured at  $^{143}\text{Nd}/^{144}\text{Nd}=0.512104\pm 140$  ( $n=2$ ) and JNdi-1 (20 ng) was measured at  $^{143}\text{Nd}/^{144}\text{Nd}=0.512102\pm 12$  ( $n=10$ ), which is in good agreement with the accepted value of JNdi-1 of 0.512115 (Tanaka et al., 2000).

## 3. Results

The Sr, Hf, and Nd isotopic composition of the M55 cruise dust samples are summarized in Table 1. Valid Sr isotopic measurements were obtained for the majority of the samples; however, Hf and Nd isotopic measurements were difficult to obtain due to the small sample size, and are therefore supplemented with measurements performed by Rickli et al. (2010).

### 3.1. Sr isotopic composition of dust

The  $^{87}\text{Sr}/^{86}\text{Sr}$  isotopic composition of the dust samples lies within the range of 0.709763 to 0.719167. A visible isotopic sorting trend is not evident, with respect to distance from source, is evident with  $^{87}\text{Sr}/^{86}\text{Sr}$  ratios (Fig. 2); however the fine-grained samples are more radiogenic than

the coarse grained samples at a given distance from source. As indicated in Fig. 2, an average shift of >400 ppm in the  $^{87}\text{Sr}/^{86}\text{Sr}$  ratio between coarse and fine fractions is found, with a coarse and fine silicate portion average  $^{87}\text{Sr}/^{86}\text{Sr}$  ratio of 0.71358 and 0.71739 respectively, consistent with a Saharan dust source (Grousset et al., 1992). The fine silicate portion of dust samples proved to be consistently more radiogenic for Sr than the coarse portions for each sampling site. The finer grained samples may contain a higher proportion of high Rb/Sr in the form of weathered particles such as clay and micas, which can explain their more radiogenic values (Stewart et al., 2001). The water-soluble samples were significantly less radiogenic than their silicate counterparts, and were much closer to the known modern  $^{87}\text{Sr}/^{86}\text{Sr}$  seawater ratio of 0.70907 (Burke, 1982). A simple mixing analysis reveals that ~70% of the Sr in the water-soluble fraction is attributable to seasalt and ~30% from dust.

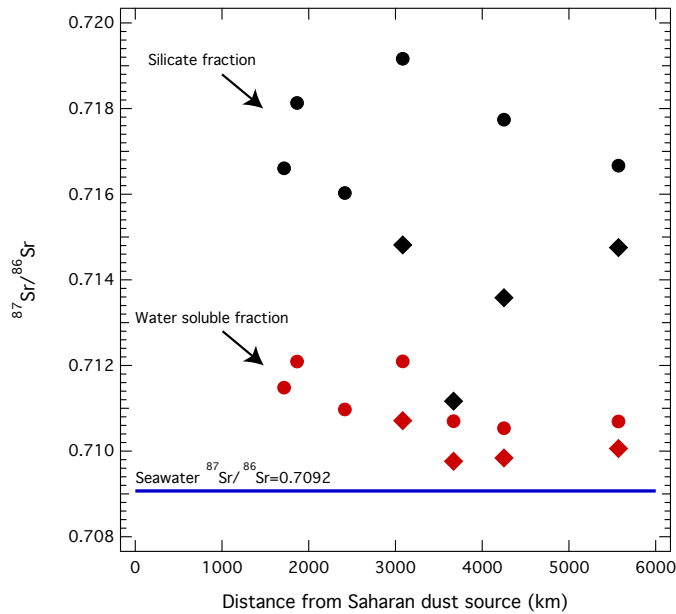


Figure 2: Strontium isotopic compositions of dust samples with respect to distance from source. Samples are separated by their size and solubility. Black circles and diamonds are fine and coarse (<1 and >1  $\mu\text{m}$  respectively) silicate fractions and red circles and diamonds are fine and coarse water-soluble fractions of dust. Modern  $^{87}\text{Sr}/^{86}\text{Sr}$  seawater ratio is plotted as dark blue line.  $2\sigma$  errors for  $^{87}\text{Sr}/^{86}\text{Sr}$  are smaller than the size of the symbols.

### 3.2. Nd and Hf isotopic compositions of dust

All Nd and Hf isotope compositions are reported here as  $\epsilon_{Nd}$  and  $\epsilon_{Hf}$ , which for Nd is defined as:

$$\epsilon_{Nd} = \left[ \frac{(^{143}\text{Nd}/^{144}\text{Nd})_{\text{sample}}}{(^{143}\text{Nd}/^{144}\text{Nd})_{\text{CHUR}}} - 1 \right] \times 10^4, \quad (1)$$

where  $(^{143}\text{Nd}/^{144}\text{Nd})_{\text{CHUR}}$  is the Nd isotopic composition of the Chondritic Uniform Reservoir (CHUR) which is  $^{143}\text{Nd}/^{144}\text{Nd} = 0.512638$  (Jacobsen and Wasserburg, 1980) and  $^{176}\text{Hf}/^{177}\text{Hf} = 0.282769$  (Nowell et al., 1998). The Nd isotopic composition of the dust samples lies within the range of  $\epsilon_{Nd}$  -12.0 to -14.1, with an average  $\epsilon_{Nd}$  of  $-13.2 \pm 0.5$  (n=8), consistent with a crustal

Saharan source (Grousset et al., 1992). There is no discernible Nd isotopic sorting trend with respect to distance from the source, however the fine fraction of samples 3, 4 and 7 have less radiogenic values than their coarse counterparts. The Nd and Sr isotopic compositions show the expected correlation in  $\epsilon_{Nd}$  versus  $^{87}\text{Sr}/^{86}\text{Sr}$  space, except for one sample which has the most radiogenic  $^{87}\text{Sr}/^{86}\text{Sr}$  value (0.719167) and also has the most radiogenic  $\epsilon_{Nd}$  value (-8.6) (Fig. 3). Combined Hf and Nd isotopic compositions of these samples correlate well and plot close to the “zircon free array” and “bulk earth” portion of the “terrestrial array” (Fig. 4a) defined by Bayon et al. (2009). These results are consistent with Rickli et al. (2010), who analyzed coarser fractions nearer to the dust storm (Table 1). The Hf isotopic composition of the dust samples varies from -8.9 to -2.5, revealing significant variations in  $\epsilon_{Hf}$  as a function of distance from the dust source, showing dust to be less radiogenic close to the source and progressively more radiogenic as distance from the source increased (Fig. 4b).

## 4. Discussion

### 4.1. Dust Provenance

Continental-derived dust that is transported throughout the atmosphere can be used as a tracer of air circulation and transport patterns (Basile et al., 1996; Grousset and Biscaye, 2005; Revel-Rolland et al., 2006; Delmonte et al., 2010). The radiogenic isotopic compositions of dust have been used in this way as a proxy for paleo-climate and atmospheric circulation on both a regional and global scale (Harrison et al., 2001). Dust deposition has been noted to have a significant impact on ecosystems, for example the deposition of desert dust on semi-arid lands encourages the development of soil (McTainsh, 1984; Tsoar and Pye, 1987; Reheis et al., 1995; Kohfeld and Harrison, 2001). Far traveled dust particles have also been attributed to provide enrichment in limiting nutrients (P, K, Mg, Na, Ca, Fe, Cu, Mn and Mo) in forest, river, lake and marine ecosystems (Reynolds et al., 2001; Okin et al., 2004; McTainsh and Strong, 2007) and are therefore capable of affecting the global carbon cycle. Variations in the provenance of dust reaching a particular location can be a valuable indicator of changes in dust production, sources, and atmospheric transport pathways through time as a function of climate change. Quantifying the effects of physical and chemical weathering, as well as the changes that take place during transport on isotopic composition, is thus important for accurately interpreting dust provenance. In particular, any changes to the dust particles that occur during transport, such as density and size related fallout, can have implications for any studies that have assumed that the composition remains constant with respect to distance from the source.

### 4.2. Sr water soluble fraction

We find that the large component of Sr (~70%) from seasalt in the water-soluble portion of the samples highlights the importance of effective sample separation between the water insoluble and soluble portions prior to isotopic analysis of dust-derived Sr (Fig. 2). Previous studies utilizing Sr isotopes to trace dust transport have neglected to separately analyze the soluble and non soluble portions of Sr-bearing materials, resulting in measured  $^{87}\text{Sr}/^{86}\text{Sr}$  values which are not an accurate representation of nutrient pools or dust sources (Jin et al., 2011). A study performed by Pett-Ridge et al. (2008) measured Sr isotopes as a tracer of weathering processes and dust inputs in a tropical watershed using a simple mass balance model to determine the proportion of radiogenic Sr leached from altered biotite. It was proposed that mineral aerosol dust deposition is a source of radiogenic Sr in the watershed system, and a flux equation was used to describe

the amount of radiogenic Sr input by dust sources (Pett-Ridge et al., 2008). The flux equation fails to take into account the quantity of sea salt contribution to the overall dust flux, which may result in inaccurate calculated Sr concentrations from dust input and characterization of sources of radiogenic Sr. Our results show that the non soluble portion of Saharan dust samples is significantly more radiogenic than the soluble portion (Fig. 2), and measurements performed without proper separation of the soluble from non soluble portion may be more representative of sea salt aerosol input rather than aerosol mineral dust.

#### 4.3. Sr and Nd detrital fraction

Past research has demonstrated that transport sorting of dust has an insignificant effect upon other radiogenic isotope tracers, such as Nd (Goldstein et al., 1984 and Frank, 2002). Our data also show that no significant isotopic variation in Sr occurs with respect to distance from the source; however, there is a significant difference in the isotopic composition between the coarse sized dust particles ( $>1 \mu\text{m}$ ) and the fine fraction ( $<1 \mu\text{m}$ ) (Fig. 2) collected at each site, which is consistent with the findings of Biscaye (1971) and Goldstein and Jacobsen (1987). The Sr isotopic differences with respect to size fraction have clear implications for dust transport studies that have primarily focused on only coarse sized particles for analysis. A previous study concerning dust provenance in Greenland ice compared possible source area samples in a  $<5 \mu\text{m}$  size fraction whereas the mean particle size of dust entrained within the ice is between  $\sim 1.6\text{-}2 \mu\text{m}$  in diameter (Steffensen, 1997). The authors determined Saharan provenance for the dust was not likely based on  $^{87}\text{Sr}/^{86}\text{Sr}$  and  $\epsilon_{\text{Nd}}$  isotope mixing plots whereas our results show that input from dust originating from the Sahara is a distinct possibility for dust found in Greenland ice (Fig. 3) (Biscaye et al., 1997). The fine fraction ( $<1 \mu\text{m}$ ) Sr and Nd isotopic compositions are in good agreement with values obtained by Lupker et al., (2010), which supports the conclusion that a significant component of the dust flux to Greenland could originate in the Sahara (Fig. 3).

#### 4.4. Nd and Hf detrital fraction

The Nd and Hf isotopic compositions measured in this study lie within the “bulk earth” and “zircon free” array (Fig. 4a) (Bayon et al., 2009). The Nd and Hf isotopic composition of earth materials can be an indicator of continental weathering (Bayon et al., 2006; Rickli et al., 2009, 2010; van de Flierdt et al., 2007), as the degree of physical weathering is directly related to the amount of unradiogenic Hf from zircons released into sinks such as ice sheets, glaciers and oceans (Piotrowski et al., 2000; van de Flierdt et al., 2002). Here we suggest that the Hf isotopic composition of deposited dust particles can provide insight into the provenance, transport distance and pathways of aerosol mineral dust.

#### 4.5. Zircon Effect in Wind Driven Dust

It has been hypothesized that Hf isotopic composition of atmospheric dust changes due to the variable loss of the high-density mineral zircon ( $\text{ZrSiO}_4$ ), as a function of distance from the source area. Hf constitutes between 1-4 weight % of the mineral zircon (Hoskin and Schaltegger, 2003), and is therefore concentrated in a single mineral phase in most silicate materials. Zircon also has a very low Lu/Hf ratio, resulting in very unradiogenic  $^{176}\text{Hf}/^{177}\text{Hf}$ , due to slow radiogenic ingrowth of  $^{176}\text{Hf}$  from decay of  $^{176}\text{Lu}$  over time (Patchett et al., 1981). The chemical indestructibility of zircon over geologic time therefore results in a low  $^{176}\text{Hf}/^{177}\text{Hf}$  ratio being imparted to the more zircon-rich parts of the sedimentary system (Vervoort et al., 1999). Physical weathering, erosion and transport processes of continental material also fractionates

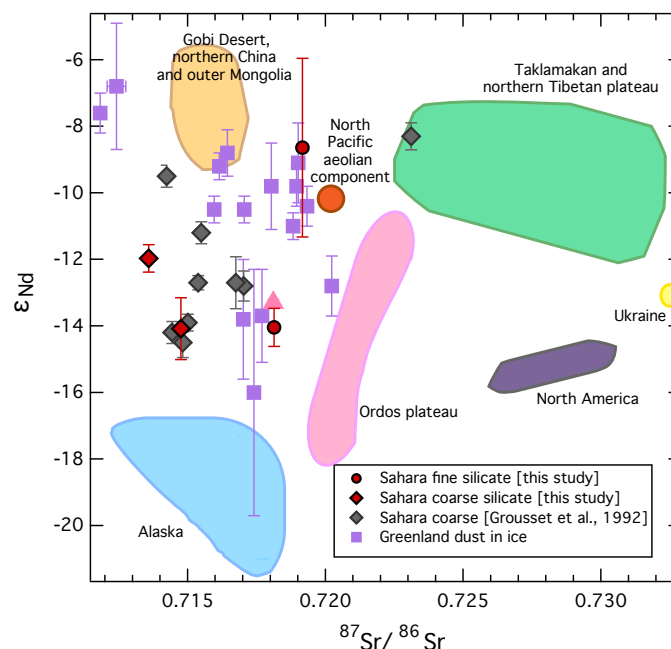


Figure 3: Sr and Nd isotopic arrays of dust samples measured in this study, dust samples within Greenland ice from studies by Biscaye et al. (1997) and Lupker et al. (2010) (dated marine isotope stage 2 and 18th century respectively), with a compilation of potential source areas (PSAs) isotopic compositions obtained from literature (Grousset et al., 1992; Biscaye et al., 1997; Kukla and Cílek, 1996; Bory et al., 2003; Kanayama et al., 2002; Stancin et al., 2006; Chen et al., 2007). Red circles and diamonds are fine and coarse (<1 and >1  $\mu\text{m}$  respectively) silicate fractions and purple squares are dust samples from Greenland ice. PSA samples are separated by color.

coarser, sandy sediments with abundant zircons from clay-sized (zircon-poor) sediments with much higher Lu/Hf (Patchett et al., 1984), resulting in more radiogenic  $^{176}\text{Hf}/^{177}\text{Hf}$  for fine clays. Additionally, preferential chemical weathering of rare earth element (REE)-bearing minerals can result in high Lu/Hf dissolved phases being more available for adsorption onto clay particles (Patchett et al., 1984).

The global Hf isotope values (seawater array) observed in the ocean have been explained by incongruent continental weathering (Piotrowski et al., 2000; van de Flierdt et al., 2002; van de Flierdt et al., 2004; Bau and Koschinsky, 2006; van de Flierdt et al., 2007; Stichel et al., 2012). In particular, preferential weathering of the non-zircon portions of the upper continental crust has been suggested to be responsible for the observed seawater array observed in Mn-crusts and nodules (Albarede et al., 1998). The concept of incongruent continental weathering can be extended to dust transport studies; more specifically, that the retention and fallout of unradiogenic Hf in zircon particles resistant to weathering will produce a disproportionate amount of variation in the observed Hf isotopic compositions of dust particles advected from a dust storm compared to other isotopic systems.



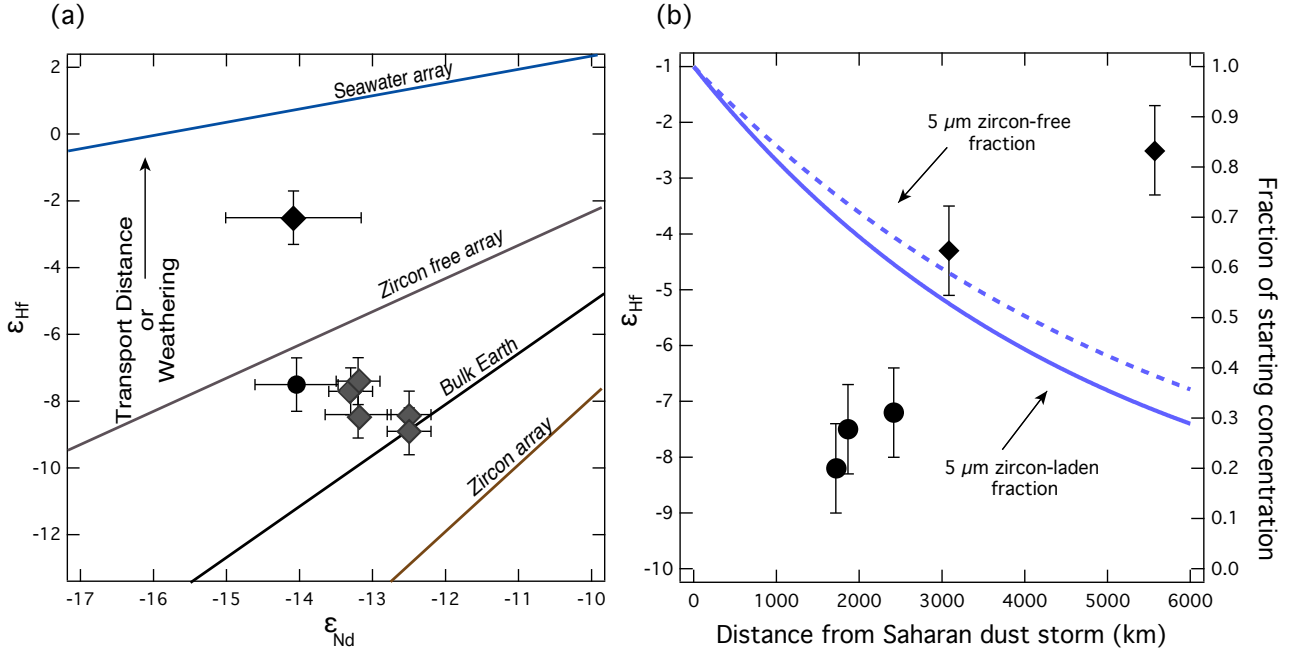


Figure 4: (a) Hf and Nd isotopic arrays of earth’s oceans, sediments and igneous rocks (compilation from Bayon et al., 2009), plotted with Hf-Nd isotope data from dust storm samples collected across the Atlantic (Table 1 this study, supplemented with data from Rickli et al., 2010). Circles and diamonds are fine and coarse ( $<1$  and  $>1 \mu\text{m}$  respectively) silicate fractions, with black symbols from this study and gray symbols from Rickli et al. (2010). (b) The trend towards less radiogenic values with distance due to zircon loss: dust Hf isotopic composition measured in this study as a function of distance from source region. Also plotted are atmospheric transport model results (derived from Fig. 5) for  $5 \mu\text{m}$  zircon-free and zircon-laden dust fraction (dashed and solid lines respectively) with a windspeed of  $12 \text{ m s}^{-1}$ .

#### 4.6. Atmospheric Transport Model: Particle Size and Density as limiting factor of “zircon effect”

The effects of physical and chemical weathering at the Earth’s surface on  $^{176}\text{Hf}/^{177}\text{Hf}$  ratios are complicated (Vervoort et al., 1999); however, we infer through transport modeling (below) that density sorting of zircon is the main factor behind the observed variability in  $^{176}\text{Hf}/^{177}\text{Hf}$  ratios. Initial entrainment of zircon-laden dust particles within dust storms is relatively small as a volume percentage due to its high density; nevertheless, it has been proposed that the high density of zircon entrained within storms of atmospheric dust will result in a systematic depletion of zircon in the dust as a function of time and distance traveled (Rickli et al., 2010). Here we confirm that prior weathering, size sorting, and dissolution occurring before dust entrainment, combined with the effects of mineral density related fallout and size sorting during transport, has a quantifiable effect on the Hf radiogenic isotope composition with distance from the source area of a large Saharan dust storm (Fig. 4b).

In our dataset, samples closer to the dust source possess more negative, less radiogenic  $\epsilon_{\text{Hf}}$  values due to their relative enrichment in zircon. Approximate relative concentrations of zircon-poor vs. zircon-laden silicate dust as a function of distance from the dust storm were calculated using a steady-state general transport model adapted from Jacobson and Holmden (2006). The

model assumes that dust is injected into the atmosphere at the coastline of Western Africa, the transport occurs along the northeasterly trade wind direction at a constant velocity, the effect of dispersion is ignored and reaction rates are first order. The dust is advected by wind and removed from the atmosphere by dry deposition, which was calculated separately for both varying sizes of dust particles. The dry deposition velocity was calculated using an equation for gravitational settling from Zhang et al. (2001). The zircon dry deposition velocity is approximately double that of the zircon-free silicate dust. The general transport equations for zircon-free versus pure zircon dust are as follows:

$$C_{atm}^{sil}(x) = C_{atm}^{sil}(o) \exp\left[-\frac{x}{v}(\lambda_{dry} + \lambda_{sil})\right] \quad (2)$$

$$C_{atm}^{zir}(x) = C_{atm}^{zir}(o) \exp\left[-\frac{x}{v}(\lambda_{dryzir} + \lambda_{zir})\right], \quad (3)$$

where  $C_{atm}^{sil}(o)$  and  $C_{atm}^{zir}(o)$  are the initial concentrations of zircon-free silicate and pure zircon dust, respectively, in a vertical column of the atmosphere at the eastern coast of the Atlantic Ocean.  $C_{atm}^{sil}(o)$  and  $C_{atm}^{zir}(o)$  are calculated using the following equation:

$$C_{atm}^i = C_{atm}^{dust}(o) f_i h_{atm}, \quad (4)$$

where  $i=sil$  or  $zir$ , and  $C_{atm}^{dust}(o)$  is the mean concentration of bulk dust in a vertical column of air at the coastline,  $f_i$  is the mass fraction of particles present in the bulk dust, and  $h_{atm}$  is the height of dust injection into the atmosphere. The distance along the transport path is represented by  $x$ , and  $v$  is the wind velocity.  $\lambda_{dryzil}$  is the dry deposition rate of silicate dust,  $\lambda_{sil}$  is the wet deposition rate of silicate dust,  $\lambda_{dryzir}$  is the dry deposition rate of zircon laden dust, and  $\lambda_{zir}$  is the wet deposition rate of zircon-laden dust. For a full description of the values used in the general transport model see Table 2.

The ‘‘zircon effect’’ is visible in the samples closer to the dust source possessing lower  $\epsilon_{Hf}$  values due to their enrichment in zircon-laden particles (Fig. 4b). The measured  $\epsilon_{Hf}$  values gradually increase (become more radiogenic) as the relative concentration of zircon-laden dust particles decreases with distance due to density related fallout. The rapid decrease in zircon content (in  $g/m^2$ ) with respect to distance from the source is reflected in model results for coarse particles ( $10 \mu m$ ) in a column of air, but not for fine particles ( $1 \mu m$ ). The coarse particle concentration of both zircon and non-zircon silicate particles decreases exponentially as the storm progresses across the Atlantic, but with the zircon particles falling out of the air column more rapidly than the silicate particles due to the effects of density (Fig. 5). In contrast, the fine fraction dust shows no difference in fallout rate between the zircon and zircon-free dust fractions. We find that the critical parameter governing fine dust fallout as a function from source area is the diameter of the particle rather than the particle density. Rather than being attributed to mineral sorting related to physical and chemical weathering at the source (along with the effects of density upon initial entrainment for transport), we find that the isotopic analysis of Hf reveals the majority of coarse zircon particles were deposited within 3000 km of the dust source, a conclusion supported by the model results presented here. As the fine dust fraction is transported from its source region the effects of density do not produce a discrepancy in proportions of zircon-laden and zircon-poor dust particles. As seen in Fig. 5,  $1 \mu m$  dust particles do not show a separate fallout rate for zircon and zircon-free fractions.

#### 4.7. Effects of variable wind speed and particle diameter

By varying the particle size in the dust transport model we have determined that particle diameters  $>1 \mu m$  show a fallout rate that is dependent upon density, which results in a visible

difference between the zircon and zircon-free fractions as a function of distance from the source (Fig. 5). We suggest that the critical particle diameter is  $5 \mu\text{m}$ , such that 3000 km from the source with a wind speed of 8 m/s there is a significant difference ( $\sim 0.1$ ) in the fraction of starting concentration between the zircon and zircon-free fractions. For dust particles  $>5 \mu\text{m}$ , the “zircon effect” should be evident in dust inputs to seawater, ice sheets, and glaciers, and we can therefore discern whether the dust source is near or far relative to its deposition site based off its Hf isotopic composition. The maximum windspeed in the Saharan air layer is often 10-17  $\text{m s}^{-1}$  and can be as high as  $25 \text{ m s}^{-1}$ , which is significantly stronger than the typical trade wind speed (Dunion and Velden, 2004). Our model results show that wind speed variation will have a significant effect upon the transport and deposition of dust particles (Fig. 5). Dust particles  $>10 \mu\text{m}$  will gravitationally settle out of the atmosphere in close proximity to their source as a function of the wind speed (Fig. 5). The difference in density between zircon and non-zircon silicate particles is still evident, however the likelihood of these particles reaching ice sheets or glaciers is small. Depending on the proximity of the source area to the ocean, the “zircon effect” may still be evident in the input to seawater as previous studies have demonstrated that close range continental weathering inputs have measurable effects upon the Hf isotopic composition of seawater (Rickli et al., 2009; Rickli et al., 2010). The resistance to weathering and subsequent insolubility of the mineral zircon may result in unradiogenic Hf isotopic compositions of insoluble dust particles suspended in seawater, but have little to no effect on the soluble Hf isotopic composition of seawater.

## 5. Conclusions

We have shown that sorting of dust particles with respect to their size, density, and susceptibility to weathering can affect the observed isotopic composition at varying distances within a dust storm from its source. Modeling the “zircon effect” related to atmospheric dust transport has the potential to differentiate near from far sources of dust particles. Modeled results show an almost complete absence of coarse zircon particles 5000 km away from the dust source. The Hf isotopic composition of dust particles of a certain size fraction can be extrapolated to represent the relative amount of zircon present in the dust sample as demonstrated in Fig. 4b. The amount of unradiogenic Hf present in the samples has the potential to reveal whether the dust was sourced from an exposed local or a transcontinental source. Understanding the causes and changes in isotopic composition of dust particles with respect to distance from the dust source to sink is essential to accurately reconstruct dust provenance, transport pathways, and the interpretation of effects of dust deposition upon the biogeochemistry of the marine and terrestrial biosphere. We suggest that a more detailed study with more dust samples and dust size fractions be carried out to determine whether there is in fact a significant difference in isotopic composition based upon small variations (on the order of  $\mu\text{m}$ ) of dust size fraction.

## 6. Acknowledgments

The samples for this research were kindly provided by A.R. Baker. This research was funded by the University of Michigan Rackham Graduate School and the Turner Award from the Department of Earth and Environmental Sciences. We would also like to thank the Radiogenic Isotope Geochemistry Laboratory at Michigan (J. Blum, director) for access to laboratory and mass spectrometer facilities.

## References

- [1] Aciego, S.M., Bourdon, B., Lupker, M., Rickli, J., 2009. A new procedure for separating and measuring radiogenic isotopes (U, Th, Pa, Ra, Sr, Nd and Hf) in ice cores. *Chemical Geology* 266 doi:10.1016/j.chemgeo.2009.06.003.
- [2] Albarede, F., Simonetti, A., Vervoort, J.D., Blichert-Toft, J., Abouchami, W., 1998. A Hf-Nd isotopic correlation in ferromanganese nodules. *Geophysical Research Letters* 25, 3895-3898.
- [3] Baker, A.R., 2004. Inorganic iodine speciation in tropical Atlantic aerosol. *Geophysical Research Letters* 31, doi:10.1029/2004GL020144.
- [4] Basile, I., Grousset, F.E., Revel, M., Petit, J.R., Biscaye, P.E., Barkov, N.I., 1997. Patagonian origin of glacial dust deposited in East Antarctica (Vostok and Dome C) during glacial stages 2, 4 and 6. *Earth and Planetary Science Letters* 146, 573-589.
- [5] Bau, M., Koschinsky, A., 2006. Hafnium and neodymium isotopes in seawater and in ferromanganese crusts: the element perspective. *Earth and Planetary Science Letters* 241, 952-961.
- [7] Bayon, G., Vigier, N., Burton, K.W., Brenot, A., Carignan, J., Etoubleau, J., Chu, N.C., 2006. The control of weathering processes on riverine and seawater hafnium isotope ratios. *Geology* 32, 433-436.
- [7] Bayon, G., Burton, K.W., Soulet, G., Vignier, N., Dennielou, B., Etoubleau, J., Ponzevera, E., German, C.R., Nesbitt, R.W., 2009. Hf and Nd isotopes in marine sediments: Constraints on global silicate weathering. *Earth and Planetary Science Letters* 277, 318-326.
- [9] Biscaye, P.E., 1971. The rubidium, strontium, strontium-isotope system in deep-sea sediments: Argentine basin. *Journal of Geophysical Research* 76, 5087-5095.
- [9] Biscaye, P.E., Grousset, F.E., Revel, M., Van der Gaast, S., Zielinski, G.A., Vaars, A., Kukla, G., 1997. Asian provenance of glacial dust (stage 2) in the Greenland Ice Sheet Project 2 Ice Core, Summit, Greenland., *Journal of Geophysical Research* 102, 765-781.
- [10] Bory, A.J.-M., Biscaye, P.E., Piotrowski, A.M., Steffensen, J.P., 2003. Regional variability of ice core dust composition and provenance in Greenland. *Geochemistry Geophysics Geosystems* 4, doi:10.1029/2003GC000627.
- [11] Burke, W.H., Denison, R.E., Hetherington, E.A., Koepnick, R.B., Nelson, H.F., Otto, J.B., 1982. Variation of seawater  $^{87}\text{Sr}/^{86}\text{Sr}$  throughout Phanerozoic time. *Geology* 10, 516-519.
- [12] Chen, J., Li, G., Yang, J., Rao, W., Lu, H., Balsam, W., Sun, Y., Ji, J., 2007. Nd and Sr isotopic characteristics of Chinese deserts: Implications for the provenances of Asian dust. *Geochimica Cosmochimica Acta* 71, 3904-3914.
- [13] Dasch, E., 1969. Strontium isotopes in weathering profiles, deep-sea sediments, and sedimentary rocks. *Geochimical et Cosmochimica Acta* 33, 1521-1552.
- [14] Delmonte, B., Baroni, C., Andersson, P.S., Schoberg, H., Hansson, M., Aciego, S., Petit, J.R., Albani, S., Mazzola, C., Maggi, V., Frezzotti, M., 2010. Aeolian dust in the Talos Dome ice core (East Antarctica, Pacific/Ross Sea sector): Victoria Land versus remote sources over the last two climate cycles. *Journal of Quaternary Science* 25, 1327-1337.
- [15] Duce, R.A., Liss, P.S., Merrill, J.T., Atlas, E.L., Buat-Menard, P., Hicks, B.B., Miller, J.M., Prospero, J.M., Arimoto, R., Church, T.M., Ellis, W., Galloway, J.N., Hansen, L., Jickells, T.D., Knapp, A.H., Reinhardt, K.H., Schneider, B., Soudine, A., Tokos, J.J., Tsunogai, S., Wollast, R., Zhou, M., 1991. The atmospheric input of trace species to the world ocean. *Global Biogeochemical Cycles* 5, 139-259.
- [16] Dunion, J.P., Velden, C.S., 2004. The Impact of the Saharan Air Layer on Atlantic Tropical Cyclone Activity. *Bulletin of the American Meteorological Society* 85, 353-365.
- [17] Frank, M., 2002. Radiogenic isotopes: tracers of past ocean circulation and erosional input. *Reviews of Geophysics* 40, 1001.
- [18] Genthon, C., 1993. Simulations of desert dust and sea-salt aerosols in Antarctica with a general model of the atmosphere. *Tellus* 44B, 371-389.
- [19] Goldstein, S.L., ONions, R.K., Hamilton, P.J., 1984. A Sm-Nd isotopic study of atmospheric dusts and particulates from major river systems. *Earth and Planetary Science Letters* 70, 221-236.
- [20] Goldstein, S.J., Jacobsen, S.B., 1987. The Nd and Sr isotopic systematics of river-water dissolved material: implications for the sources of Nd and Sr in seawater. *Chemical Geology* 66, 245-272.
- [21] Grousset, F.E., Rognon, P., Coude-Gaussen, G., Pedemay, P., 1992. Origins of peri-Saharan dust deposits traced by their Nd and Sr isotopic composition. *Palaeogeography, Palaeoclimatology, Palaeoecology* 93, 203-212.
- [22] Grousset, F., Biscaye, P., 2005. Tracing dust sources and transport patterns using Sr, Nd and Pb isotopes. *Chemical Geology* 222, 149-167.
- [23] Harrison, S.P., Kohfeld, K.E., Roelandt, C., Claquin, T., 2001. The role of dust in climate changes today, at the last glacial maximum and in the future. *Earth-Science Reviews* 54, 43-80.
- [24] Hoskin, P.W.O., Schaltegger, U., 2003. The composition of zircon and igneous and metamorphic petrogenesis. *Reviews in Mineralogy and Geochemistry.-Zircon* 53, 27-62.
- [25] Jacobsen, S.B., Wasserburg, G.J., 1980. Sm-Nd isotopic evolution of chondrites. *Earth and Planetary Science Letters* 50, 139-155.

- [26] Jacobson, A.D., Holmden, C., 2006. Calcite dust and the atmospheric supply of Nd to the Japan Sea. *Earth and Planetary Science Letters* 244, 418-430.
- [27] Jickells, T.D., An, Z.S., Andersen, K.K., Baker, A.R., Bergametti, G., Brooks, N., Cao, J.J., Boyd, P.W., Duce, R.A., Hunter, K.A., Kawahata, H., Kubilay, N., laRoche, J., Liss, P.S., Mahowald, N., Prospero, J.M., Ridgwell, A.J., Tegen, I., Torres, R., 2005. Global iron connections between desert dust, ocean biogeochemistry, and climate. *Science* 308, 67-71.
- [28] Jin, Z., You, C.-F., Yu, J., Wu, L., Zhang, F., Liu, H.-C., 2011. Seasonal contributions of catchment weathering and eolian dust to river water chemistry, northeastern Tibetan Plateau: Chemical and Sr isotopic constraints. *Journal of Geophysical Research* 116, doi:10.1029/2011JF002002.
- [29] Joussaume, S., 1993. Paleoclimatic tracers: An investigation using an atmospheric general circulation model under ice age conditions. *Journal of Geophysical Research* 98, 2767-2805.
- [30] Kanayama, S., Yabuki, S., Zeng, F.J., Liu, M.Z., Shen, Z.B., Liu, L.C., Yanagisawa, F., Abe, O., 2005. Size-dependent geochemical characteristics of Asian dust - Sr and Nd isotope compositions as tracers for source identification. *Journal of the Meteorological Society of Japan* 83A, 107-120.
- [31] Kohfeld, K., Harrison, S., 2001. DIRTMAP: the geological record of dust. *Earth-Science Reviews* 54, 81-114.
- [32] Kukla, G., Cifek, V., 1996. Plio-Pleistocene megacycles: record of climate and tectonics. *Palaeogeography, Palaeoclimatology, Palaeoecology* 120, 171-194.
- [33] Lupker, M., Aciego, S.M., Bourdon, B., Schwander, J., Stocker, T.F., 2010. Isotopic tracing (Sr, Nd, U and Hf) of continental and marine aerosols in an 18th century section of the Dye-3 ice core (Greenland). *Earth and Planetary Science Letters* 295, 277-286.
- [35] McTainsh, G.H., 1984. The nature and origin of the aeolian mantles of central northern Nigeria. *Geoderma* 33, 13-37.
- [35] McTainsh, G., Strong, C., 2007. The role of aeolian dust in ecosystems. *Geomorphology* 89, 39-54.
- [36] Nowell, G.M., Kempton, P.D., Noble, S.R., Fitton, J.G., Saunders, A.D., Mahoney, J.J., Taylor, R.N., 1998. High precision Hf isotope measurements of MORB and OIB by thermal ionisation mass spectrometry: insights into the depleted mantle. *Chemical Geology* 149, 211-233.
- [37] Okin, G.S., Mahowald, N., Chadwick, O.A., Artaxo, P., 2004. Impact of desert dust on the biogeochemistry of phosphorus in terrestrial ecosystems. *Global Biogeochemical Cycles* 18, doi:10.1029/2003GB002145.
- [39] Patchett, P.J., Kouvo, O., Hedge, C.E., Tatsumoto, M., 1981. Evolution of Continental Crust and Mantle Heterogeneity: Evidence from Hf Isotopes. *Contributions to Mineralogy and Petrology* 78, 279-297.
- [39] Patchett, P.J., White, W.M., Feldmann, H., Kielinczuk, S., Hoffmann, A.W., 1984. Hafnium/rare earth element fractionation in the sedimentary system and crustal recycling into the Earth's mantle. *Earth and Planetary Science Letters* 69, 365-378.
- [40] Pett-Ridge, J.C., Derry, L.A., Kurtz, A.C., 2008. Sr isotopes as a tracer of weathering processes and dust inputs in a tropical granitoid watershed, Luquillo Mountains, Puerto Rico. *Geochimica et Cosmochimica Acta* 73, 25-43.
- [41] Piotrowski, A.M., Lee, D.-C., Christensen, J.N., Burton, K.W., Halliday, A.N., Hein, J.R., Gunther, D., 2000. Changes in erosion and ocean circulation recorded in the Hf isotopic compositions of North Atlantic and Indian Ocean ferromanganese crusts. *Earth and Planetary Science Letters* 181, 315-325.
- [42] Prospero, J.M., 1999. Long-range transport of mineral dust in the global atmosphere: Impact of African dust on the environment of the southeastern United States. *Proceedings of the National Academy Sciences of the United States of America* 96, 3396-3403.
- [43] Reheis, M.C., Kihl, R., 1995. Dust deposition in southern Nevada and California, 1984-89: relations to climate, source area, and source lithology. *Journal of Geophysical Research* 100, 8893-8918.
- [44] Revel-Rolland, M., De Deckker, P., Delmonte, B., Hesse, P.P., Magee, J.W., Basile-Doelsch, I., Grousset, F., Bosch, D., 2006. Eastern Australia: A possible source of dust in East Antarctica interglacial ice. *Earth and Planetary Science Letters* 249, 1-13.
- [45] Reynolds, R., Belnap, J., Reheis, M., Lamothe, P., Luiszer, F., 2001. Aeolian dust in Colorado Plateau soils: nutrient inputs and recent change in source. *Proceedings of the National Academy Sciences of the United States of America* 98, 7123-7127.
- [47] Rickli, J., Frank, M., Halliday, A.N., 2009. The hafnium-neodymium isotopic composition of Atlantic seawater. *Earth and Planetary Science Letters* 280, 118-127.
- [47] Rickli, J., Frank, M., Baker, A.R., Aciego, S., de Souza, G., Georg, R.B., Halliday, A.N., 2010. Hafnium and neodymium isotopes in surface waters of the eastern Atlantic Ocean: Implications for sources and inputs of trace metals to the ocean. *Geochimica et Cosmochimica Acta* 74, 540-557.
- [48] Sarthein, M., Tetzlaff, G., Koopmann, B., Wolter, K., Pflaumann, U., 1981. Glacial and interglacial wind regimes over the eastern subtropical Atlantic and north-west Africa. *Nature* 293, 193-196.
- [49] Shinn, E.A., Smith, G.W., Prospero, J.M., Betzer, P., Hayes, M.L., Garrison, V., Barber, R.T., 2000. African dust and the demise of Caribbean coral reefs. *Geophysical Research Letters* 27, 3029-3032.
- [50] Stancin, A.M., Gleason, J.D., Rea, D.K., Owen, R.M., Moore Jr., T.C., Blum, J.D., Hovan, S.A., 2006. Radiogenic

- isotopic mapping of late Cenozoic eolian and hemipelagic sediment distribution in the east-central Pacific. *Earth and Planetary Science Letters* 248, 840-850.
- [51] Steffensen, J.P., 1997. The size distribution of microparticles from selected segments of the Greenland Ice Core Project ice core representing different climatic periods. *Journal Geophysical Research* 102, 755-763.
- [52] Stewart, B.W., Capo, R.C., Chadwick, O.A., 2001. Effects of rainfall on weathering rate, base cation provenance, and Sr isotope composition of Hawaiian soils. *Geochimica et Cosmochimica Acta* 65, 1087-1099.
- [53] Stichel, T., Frank, M., Rickli, J., Haley, B.A., 2012. The hafnium and neodymium isotope composition of seawater in the Atlantic sector of the Southern Ocean. *Earth and Planetary Science Letters* 317-318, 282-294.
- [54] Tanaka, T., Togashi, S., Kamioka, H., Amakawa, H., Kagami, H., Hamamoto, T., Yuhara, M., Orihashi, Y., Yoneda, S., Shimizu, H., Kunimaru, T., Takahashi, K., Yanagi, T., Nakano, T., Fujimaki, H., Shinjo, R., Asahara, Y., Tanimizu, M., Dragusanu, C., 2000. JNdi-1: a neodymium isotopic reference in consistency with LaJolla neodymium. *Chemical Geology* 168, 279-281.
- [55] Tsoar, H., Pye, K., 1987. Dust transport and the question of desert loess formation. *Sedimentology* 34, 139-154.
- [58] van de Flierdt, T., Frank, M., Lee, D.-C., Halliday, A.N., Reynolds, B.C., Hein, J.R., 2002. Glacial weathering and the hafnium isotope composition of seawater. *Earth and Planetary Science Letters* 201, 639-647.
- [58] van de Flierdt, T., M. Frank, Halliday, A.N., Hein, J.R., Hattendorf, B., Gunther, D., Kubik, P.W., 2004. Tracing the history of submarine hydrothermal inputs and the significance of hydrothermal hafnium for the seawater budget-A combined Pb-Hf-Nd isotope approach. *Earth and Planetary Science Letters* 222, 259-273.
- [58] van de Flierdt, T., Goldstein, S.L., Hemming, S.R., Roy, M., Frank, M., Halliday, A.N., 2007. Global neodymium-hafnium isotope systematics-revisited, *Earth and Planetary Science Letters* 259, 432-441.
- [59] Vervoort, J.D., Patchett, P.J., Blichert-Toft, J., Albarede, F., 1999. Relationships between Lu-Hf and Sm-Nd isotopic systems in the global sedimentary system. *Earth and Planetary Science Letters* 168, 79-99.
- [60] Watson, A.J., Bakker, D.C.E., Ridgwell, A.J., Boyd, P.W., Law, C.S., 2000. Effect of iron supply on Southern Ocean CO<sub>2</sub> uptake and implications for glacial atmospheric CO<sub>2</sub>. *Nature* 407, 730-733.
- [61] Weis, D., Kieffer, B., Hanano, D., Silva, L., Barling, J., Pretorius, W., Maerschalk, C., Mattielli, N., 2007. Hf isotope compositions of US Geological Survey reference materials. *Geochemistry, Geophysics, Geosystems* 8.
- [62] Zhang, L., Gong, S., Padro, J., Barrie, L., 2001. A size-segregated particle dry deposition scheme for an atmospheric aerosol module. *Atmospheric Environment* 35, 549-560.

Table 1: Strontium, hafnium and neodymium isotopic compositions of dust samples collected during cruise M55. *F* and *C* denote fine and coarse grained samples respectively whereas *S* and *W* denote silicate and water soluble samples respectively.

Sample	date	start position	~source distance (km)	$^{87}\text{Sr}/^{86}\text{Sr} \pm 2\sigma 10^{-6}$	$^{176}\text{Hf}/^{177}\text{Hf} \pm 2\sigma 10^{-6}$	$\epsilon_{\text{Hf}} \pm 2\sigma$	$^{143}\text{Nd}/^{144}\text{Nd} \pm 2\sigma 10^{-6}$	$\epsilon_{\text{Nd}} \pm 2\sigma$
3FS	15/10/02	11.0° N, 58.7° W	5570	0.716669 (31)				
3FW	15/10/02	11.0° N, 58.7° W	5570	0.710693 (74)				
3CS	15/10/02	11.0° N, 58.7° W	5570	0.714756 (29)	0.282698 (22)	-2.5 (0.8)	0.511916 (48)	-14.1 (0.9)
3CW	15/10/02	11.0° N, 58.7° W	5570	0.710061 (15)				
4FS	17/10/02	10.6° N, 53.7° W	5130					
4CS	17/10/02	10.6° N, 53.7° W	5130				0.511966 (43)	-13.1 (0.9)
7FS	20/10/02	10.0° N, 44.8° W	4250	0.717743 (44)				
7FW	20/10/02	10.0° N, 44.8° W	4250	0.710534 (39)				
7CS	20/10/02	10.0° N, 44.8° W	4250	0.713584 (36)			0.512024 (21)	-12.0 (0.4)
7CW	20/10/02	10.0° N, 44.8° W	4250	0.709842 (13)				
9FW	22/10/02	10.0° N, 39.0° W	3669	0.710698 (37)				
9CS	22/10/02	10.0° N, 39.0° W	3669	0.711167 (21)				
9CW	22/10/02	10.0° N, 39.0° W	3669	0.709763 (19)				
11FS	24/10/02	10.0° N, 33.3° W	3083	0.719167 (24)				
11FW	24/10/02	10.0° N, 33.3° W	3083	0.712097 (22)				
11CS	24/10/02	10.0° N, 33.3° W	3083	0.714815 (65)	0.282647 (22)	-4.3 (0.8)		
11CW	24/10/02	10.0° N, 33.3° W	3083	0.710713 (16)				
20FS	02/11/02	8.4° N, 24.6° W	2415	0.716028 (23)	0.282565 (22)	-7.2 (0.8)		
20FW	02/11/02	8.4° N, 24.6° W	2415	0.710975 (17)				
20CS <sup>a</sup>	02/11/02	8.4° N, 24.6° W	2415		0.281943 (20)	-7.7 (0.7)	0.511956 (15)	-13.3 (0.3)
20CS <sup>a</sup>	replicate	8.4° N, 24.6° W	2415		0.281943 (20)	-7.4 (0.7)	0.511956 (15)	-13.2 (0.3)
24FS	06/11/02	10.9° N, 17.1° W	1715	0.716606 (37)				
24FW	06/11/02	10.9° N, 17.1° W	1715	0.711483 (23)	0.282537 (22)			
24CS <sup>a</sup>	06/11/02	10.9° N, 17.1° W	1715		0.281923 (20)	-8.4 (0.7)	0.511961 (23)	-13.2 (0.45)
25FS	07/11/02	11.0° N, 19.0° W	1864	0.718134 (20)	0.282557 (22)	-7.5 (0.8)	0.511918 (29)	-14.0 (0.6)
25FW	07/11/02	11.0° N, 19.0° W	1864	0.712092 (15)				
25CS <sup>a</sup>	08/11/02	11.0° N, 19.0° W	1864		0.281909 (20)	-8.9 (0.7)	0.511997 (15)	-12.5 (0.3)

(a) Rickli et al., 2010.

Table 2: Parameters for the atmospheric transport model.

Parameter	Description	Units
<i>Input</i>		
$x$	Distance along transport path	m
$v^a$	Wind velocity	8 m s <sup>-1</sup>
$h_{atm}^b$	Height of dust injection into the atmosphere	4 x 10 <sup>3</sup> m
$f_{sil}^c$	Mass fraction of silicate in bulk dust	0.64
$f_{zir}^d$	Mass fraction of zircon in bulk dust	0.0001
$C_{atm}^{dust}(i)^e$	Atmospheric concentration of bulk dust at x=0	4.0 x 10 <sup>-3</sup> g m <sup>-3</sup>
$C_{atm}^{sil}(i)$	Atmospheric concentration of silicate dust of $h_{atm}$ at x=0	10.24 g m <sup>-2</sup>
$C_{atm}^{zir}(i)$	Atmospheric concentration of zircon dust of $h_{atm}$ at x=0	1.6 x 10 <sup>-3</sup> g m <sup>-2</sup>
$\lambda_{drysil}^b$	Dry deposition rate for silicate dust	2.3 x 10 <sup>-8</sup> -2.0 x 10 <sup>-6</sup> s <sup>-1</sup>
$\lambda_{sil}^b$	Wet deposition rate for silicate dust	1.58 x 10 <sup>-6</sup> s <sup>-1</sup>
$\lambda_{dryzir}^b$	Dry deposition rate for zircon dust	4.33 x 10 <sup>-8</sup> -3.75 x 10 <sup>-6</sup> s <sup>-1</sup>
$\lambda_{zir}^b$	Wet deposition rate for zircon dust	1.58 x 10 <sup>-6</sup> s <sup>-1</sup>
$v_{dry}^f$	Dry deposition velocity for silicate dust	9.21 x 10 <sup>-5</sup> -8.0 x 10 <sup>-3</sup> m s <sup>-1</sup>
$v_{zir}^f$	Dry deposition velocity for zircon dust	1.73 x 10 <sup>-4</sup> -1.5 x 10 <sup>-2</sup> m s <sup>-1</sup>
<i>Output</i>		
$C_{atm}^{sil}(x)$	Atmospheric concentration of silicate dust over $h_{atm}$ at x	g m <sup>-2</sup>
$C_{atm}^{zir}(x)$	Atmospheric concentration of zircon dust over $h_{atm}$ at x	g m <sup>-2</sup>

(a) Jones et al., 2003, (b) Jacobson and Holmden, 2006, (c) Kandler et al., 2006, (d) Vervoort et al., 1999, (e) Ganor and Mamane, 1982, (f) Zhang et al., 2001.



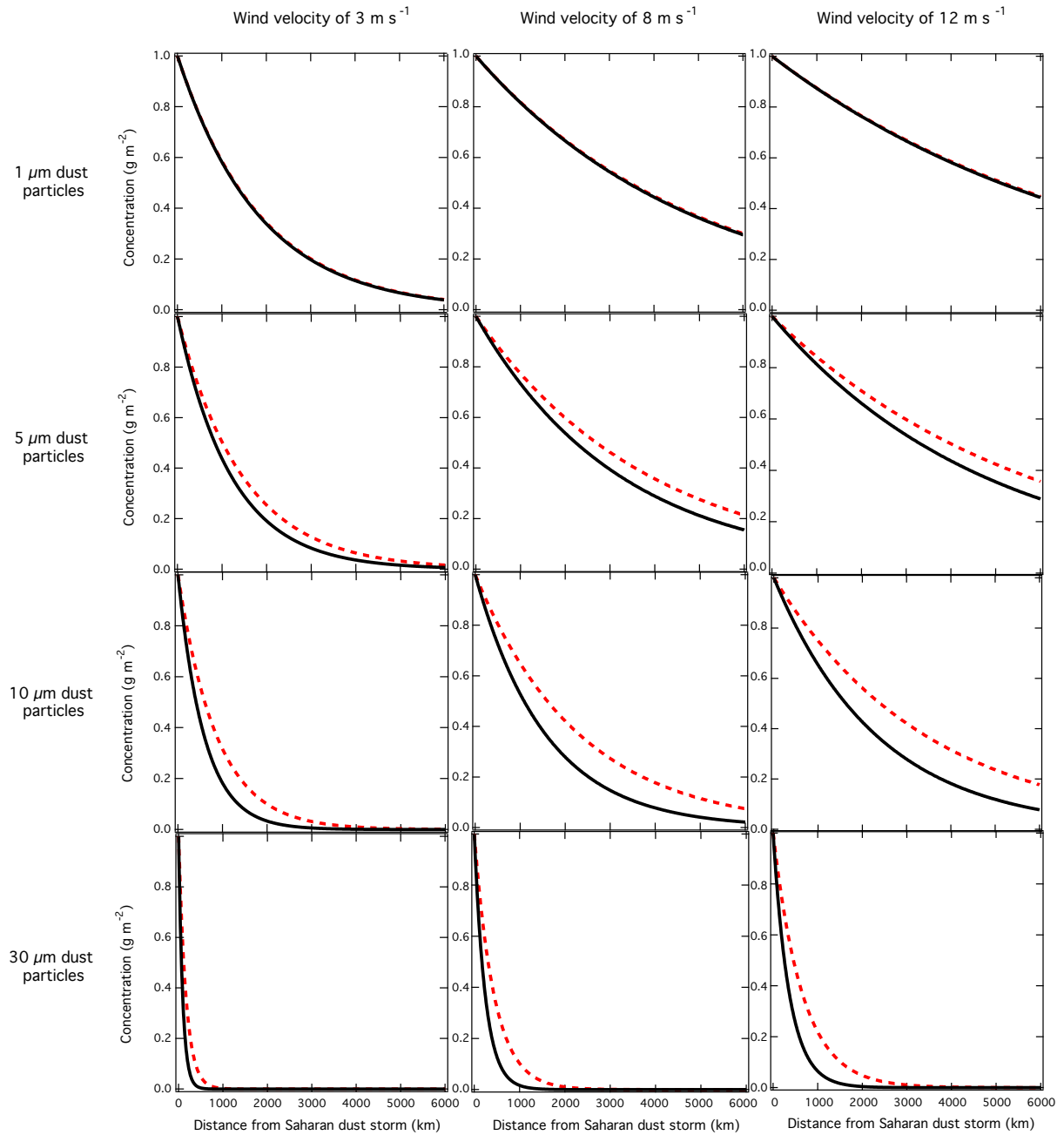


Figure 5: Atmospheric transport model results for variable dust particle diameters and windspeeds. Non zircon and zircon-laden dust fractions are represented by red dashed line and solid black line respectively. Realistic dust particle diameters vary from 1, 5, 10 and 30  $\mu\text{m}$ , which are represented here. Wind speeds vary between 3, 8 and 12  $\text{m s}^{-1}$ , however according to model simulations, seasonal wind speeds may exceed 10  $\text{m s}^{-1}$  (Jones et al., 2003).